Rank-based Bayesian variable selection for genome-wide transcriptomic analyses

Emilie Eliseussen¹ Thomas Fleischer² Valeria Vitelli¹

¹Oslo Centre for Biostatistics and Epidemiology, Department of Biostatistics, University of Oslo, Oslo, Norway ²Department of Cancer Genetics, Institute for Cancer Research, Oslo University Hospital, Oslo, Norway

E-mail: e.e.odegaard@medisin.uio.no

May 28, 2022

Abstract

Variable selection is crucial in high-dimensional omics-based analyses, since it is biologically reasonable to assume only a subset of non-noisy features contributes to the data structures. However, the task is particularly hard in an unsupervised setting, and a priori ad hoc variable selection is still a very frequent approach, despite the evident drawbacks and lack of reproducibility. We propose a Bayesian variable selection approach for rank-based transcriptomic analysis. Making use of data rankings instead of the actual continuous measurements increases the robustness of conclusions when compared to classical statistical methods, and embedding variable selection into the inferential tasks allows complete reproducibility. Specifically, we develop a novel extension of the Bayesian Mallows model for variable selection that allows for a full probabilistic analysis, leading to coherent quantification of uncertainties. We test our approach on simulated data using several data generating procedures, demonstrating the versatility and robustness of the method under different scenarios. We then use the novel approach to analyse genome-wide RNAseq gene expression data from ovarian cancer samples: several genes that affect cancer development are correctly detected in a completely unsupervised fashion, showing the method usefulness in the context of signature discovery for cancer genomics. Moreover, the possibility to also perform uncertainty quantification plays a key role in the subsequent biological investigation.

Keywords: Bayesian inference; variable selection; high-dimensional data; Mallows model; rankings; RNAseq patient data.

1. Introduction

Over the last decades, technological advances have generated an explosion of data in a variety of fields. High-throughput technologies have made -omics data more accessible to researchers, allowing for a systematic exploration of the genetic and epigenetic basis of cancer. However, -omics data pose several significant analytic challenges, including high dimensionality, high complexity and non-normality. Thus, standard statistical approaches are not applicable. To overcome these complications in high-dimensional omics-based analyses, it is considered biologically reasonable to assume that only a small piece of information is relevant for prediction or subtyping [3, 13, 14] so that a low-dimensional solution can also lead to better results interpretability. However, a frequent approach to variable selection for -omics applications consists in performing a priori ad hoc selection of genes according to in-sample statistics or outer literature information, a strategy that heavily affects the results' solidity and reproducibility [15]. Moreover, it has been established in the last decades, with the explosion of high-dimensional data methods, that variable selection should be performed jointly with the main inferential tasks, to properly estimate the uncertainties and the impact of selection on inference results [8]. Due to the unsupervised problem of variable selection for -omics data, Bayesian model-based methods are highly suitable for uncertainty propagation. While unsupervised methods may lead to inaccurate estimates because of the low signal-to-noise ratio [16], especially for high throughput genomic data, the Bayesian approach allows for incorporating prior biological knowledge when estimating relevant genes from the data. Current methods for Bayesian variable selection for high-dimensional unsupervised problems include probabilistic sparse principal component analysis [2,7], and Bayesian graphical structure learning [19,21], all with applications to -omics data.

Converting continuous data to rankings and then performing rank-based analyses is a practice that has gained much popularity in statistical genomics [10]. Different -omics data layers can have incomparable absolute scales, and the use of ranks leads to robust inference [1]. Moreover, analyzing rankings instead of continuous variables allows for easy integration of multiple heterogeneous data, and enhances the reproducibility and interpretability of results. The analysis of rank and preference data has recently seen a growing interest in the machine learning community [4], with the Plackett-Luce [24, 27] and Mallows model [25] being among the most commonly used models. The Mallows is an exponential family-type model on the permutations space, where the probability density depends on a distance between rankings. Compared to Plackett-Luce, the Mallows model shows greater flexibility in the choice of distance between permutations and is versatile in adapting to different kinds of data. As a probabilistic model for rank data, the Mallows model enjoys great interpretability, model compactness, inference and computational efficiency. Our current work is based on the Bayesian Mallows Model proposed in [31], whose implementing solution, BayesMallows, is described in [28]: BayesMallows already provides an inferential and computationally feasible approach for the most important right-invariant metrics¹, and it shows good accuracy when compared to competitors on datasets of moderate size [22]. However, for this method to be applicable to the common data dimensions in -omics applications, variable selection is crucial. Moreover, from a purely modeling perspective, imposing the Mallows data generating process on the full (genome-wide) ranked list of genes seems highly unrealistic: RNAseq measurements of moderately expressed genes tend to be very noisy, thus making a low-dimensional solution more suited to this kind of data. Imposing a ranking model only on a selection of genes allows focusing on consistently highly expressed genes since those will be selected as highly ranked items, which allows detecting genome-wide high-quality signals in a more robust way. More generally, this leads to an unsupervised variable selection procedure that can learn from the available rankings to distinguish relevant items from background ones in a high-dimensional setting, as well as provide an estimate of the position in the ranking of the selected relevant items.

The aim of this paper is to develop a novel extension of the Bayesian Mallows model providing a low-dimensional solution for variable selection in highdimensional settings. To the best of our knowledge, the only proposal similar in scope to ours is [35] which propose a partition-Mallows model (PAMA) for rank aggregation that can distinguish relevant items, as well as ranking the relevant ones. This method can handle partial lists, incorporate any available covariate information and can estimate the quality of rankers, as it is based on BARD [10] which assigns aggregated ranks based on the posterior probability that a certain item is relevant. However, PAMA only considers the Kendall distance for the Mallows model, thus allowing the partition function to have a closed form, to avoid computational issues related to the model estimation. The Bayesian Mallows model can on the other hand use any distance. Additionally, PAMA is unable to perform individual-level inference which is a typical advantage of the Bayesian Mallows model. A relatively complete simulation study is also provided, but it omits larger data examples. The recent work by [9] converts microbiome data to rankings and develops a Bayesian variable selection model using ranks to identify covariates for modeling outcome. However, common for both of these methods is the lack of applicability to high-dimensional settings, as all data examples are of much smaller dimensions compared to the typical dimension of -omics data ($> 10^4$). Other Bayesian implementations to analyse rank data have been proposed to reduce computational burden [18, 33, 34], to merge rankings from multiple sources [10, 17], and to combine rank data with other types of data [5].

The remainder of the paper is laid out as follows: in Section 2 we describe the novel Bayesian Mallows model with variable selection, and its computational implementation. Several simulation studies are described in Section 3, aimed at demonstrating the versatility and robustness of the novel method under different scenarios. In Section 4, we present an application of this modeling approach to

¹A right-invariant metric $d(\cdot, \cdot)$ is such that, for any $r_1, r_2 \in \mathcal{P}_n$, it holds: $d(r_1, r_2) = d(r_1 r_2^{-1}, \mathbf{1}_n)$, $\mathbf{1}_n = \{1, 2, ..., n\}$ [11]

RNAseq gene expression data from ovarian cancer patients. We conclude with a brief summary and discussion in Section 5.

2. Lower-dimensional Bayesian Mallows Model

We briefly present the Bayesian Mallows model (BMM) for complete data as presented in [31] in Section 2.1, and outline its extension for variable selection, the Lower-dimensional Bayesian Mallows Model (lowBMM) in Section 2.2. A description for the inference procedure can be found in Section 2.3 and Section 2.4 describes the off-line estimation of the scale parameter α .

2.1. Bayesian Mallows model for complete data

Consider a set of n items denoted as $\mathcal{A} = \{A_1, A_2, ..., A_n\}$. We assume that all n items are ranked according to a specified feature by N assessors, thus providing complete rankings $\mathbf{R}_j = \{R_{1j}, R_{2j}, ..., R_{nj}\}, j = 1, ..., N$. The Mallows model [25] is a probabilistic model for rankings defined on the space \mathcal{P}_n of permutations of dimension n, taking the form $P(r|\alpha, \rho) = \frac{1}{Z_n(\alpha, \rho)} \exp\{-\frac{\alpha}{n}d(r, \rho)\}1_{\mathcal{P}_n}(r)$, where α is a scale parameter, $\rho \in \mathcal{P}_n$ is the latent consensus ranking, $Z_n(\alpha, \rho)$ is the partition function, $1_S(\cdot)$ is the indicator of the set S, and $d(r, \rho)$ is a distance between r and ρ .

Several possibilities for the distance function exist, such as the footrule distance, the Spearman distance, and the Kendall distance. In this paper, we choose the footrule distance, which is defined as $d(\mathbf{r}, \boldsymbol{\rho}) = \sum_{i=1}^{n} |r_i - \rho_i|$: the choice of this distance is motivated by its computational efficiency, and because the equivalent of the ℓ_1 between continuous data seems more suited to genomics applications. Since the footrule distance is right-invariant, the partition function $Z_n(\alpha, \boldsymbol{\rho})$ is independent of $\boldsymbol{\rho}$ and only dependent on α . Moreover, we assume in the remainder of the paper that α is fixed and known, and we provide strategies to tune this parameter off-line. This simplifies the inferential procedure quite substantially because we can assume $Z_n(\alpha)$ to be known. For simplicity, we also do not consider clustering or missing data in the paper.

The likelihood associated to the observed rankings $\mathbf{R}_1, \dots, \mathbf{R}_N$ under the Mallows model is therefore:

$$P(\mathbf{R}_1, ..., \mathbf{R}_N | \boldsymbol{\rho}) = \frac{1}{Z_n(\alpha)} \exp \left\{ -\frac{\alpha}{n} \sum_{j=1}^N d_n(\mathbf{R}_j, \boldsymbol{\rho}) \right\} \prod_{j=1}^N 1_{\mathcal{P}_n}(\mathbf{R}_j).$$

Here $d_n(\cdot,\cdot)$ denotes the distance computed on the complete set of items. In order to use the Bayesian version of this model as introduced in [31], we need to specify a prior for ρ . In this paper, we set a uniform prior $\pi(\rho) = \frac{1}{n!} 1_{\mathcal{P}_n}(\rho)$ in the space \mathcal{P}_n of *n*-dimensional permutations. The posterior distribution for

 ρ then becomes

$$P(oldsymbol{
ho}|oldsymbol{R}_1,...,oldsymbol{R}_N) \propto rac{\pi(oldsymbol{
ho})}{Z_n(lpha)^N} \exp \left\{-rac{lpha}{n} \sum_{i=j}^N d_n(oldsymbol{R}_j,oldsymbol{
ho})
ight\}.$$

To perform inference, [31] proposed a Markov Chain Monte Carlo (MCMC) algorithm based on a Metropolis-Hastings scheme (see [28] for details on the implementation).

2.2. Lower-dimensional Bayesian Mallows model (lowBMM) for variable selection

We define $\mathcal{A}^* = \{A_1, ..., A_{n^*}\}$ as an n^* -dimensional reduced set of items, with $n^* << n$, $\mathcal{A}^* \subset \mathcal{A}$ and we assume that n^* is fixed and known. When defining the lower-dimensional Bayesian Mallows model, the underlying assumption is that only a portion of the data follows the Mallows distribution, while the rest is unranked: this is a very realistic assumption, especially in the large n setting. Items in \mathcal{A}^* are then such that $R_j|_{\mathcal{A}^*}$, $j=1,\ldots,N$, follows a Mallows model over the permutation space of dimension n^* , where with the notation $R_j|_S$ we indicate the restriction of a n-dimensional ranking to only the items belonging to the set S, which is also a ranking in dimension |S|. The remaining items in $\mathcal{A} \setminus \mathcal{A}^*$ are simply irrelevant to the scopes of the analysis, and therefore show no specific pattern in the data. This is equivalent to saying that we assume $R_j|_{\mathcal{A} \setminus \mathcal{A}^*}$, $j=1,\ldots,N$, is uniformly distributed over the space of permutations of dimension $n-n^*$.

 \mathcal{A}^* is therefore the novel model parameter characterising the variable selection setting for the Bayesian Mallows model. When n^* is fixed, the likelihood of the variable selection for the Bayes Mallows model is thus

$$P(\mathbf{R}_1, ..., \mathbf{R}_N | \boldsymbol{\rho}, \mathcal{A}^*) = \frac{1}{Z_{n^*}(\alpha)} \exp \left\{ -\frac{\alpha}{n^*} \sum_{j=1}^N d_{\mathcal{A}^*}(\mathbf{R}_j, \boldsymbol{\rho}) \right\} \prod_{j=1}^N \left\{ U_{\mathcal{A} \setminus \mathcal{A}^*}(\mathbf{R}_j) 1_{\mathcal{P}_n}(\mathbf{R}_j) \right\}$$

where $d_{\mathcal{A}^*}(\mathbf{R}_j, \boldsymbol{\rho}) := d_{n^*}(\mathbf{R}_j|_{\mathcal{A}^*}, \boldsymbol{\rho}|_{\mathcal{A}^*})$. This is the same distance as $d_n(\cdot, \cdot)$ but restricted to the n^* -dimensional set of items included in \mathcal{A}^* . The two vectors $\mathbf{R}_j|_{\mathcal{A}^*}$ and $\boldsymbol{\rho}|_{\mathcal{A}^*}$ are restrictions of \mathbf{R}_j and $\boldsymbol{\rho}$ to the set \mathcal{A}^* : they thus define a partial ordering from which an n^* -dimensional permutation can be derived. Moreover, U_S is the uniform distribution over the domain S, meaning that the term $U_{\mathcal{A}\setminus\mathcal{A}^*}(\mathbf{R}_j)$ refers to the assumption that $\mathbf{R}_j|_{\mathcal{A}\setminus\mathcal{A}^*}$ includes only noisy unranked data

Since the inferential approach is Bayesian, we have to decide priors for all parameters. As we did previously, we set a uniform prior on $\boldsymbol{\rho}$, however restricted to the n^* -dimensional space of permutations of elements of \mathcal{A}^* : $\pi(\boldsymbol{\rho}|\mathcal{A}^*) = \frac{1}{n^*!} 1_{\mathcal{P}_{n^*}}(\boldsymbol{\rho})$. We also set a uniform prior for \mathcal{A}^* over \mathcal{C} , $\pi(\mathcal{A}^*) = \frac{1}{|\mathcal{C}|} 1_{\mathcal{C}}(\mathcal{A}^*)$, where we define \mathcal{C} as the collection of all $\binom{n}{n^*}$ possible sets of dimension n^*

chosen from a set of dimension n. The posterior distribution of the variable selection for the Bayes Mallows model can then be written as

$$P(\boldsymbol{\rho}, \mathcal{A}^* | \mathbf{R}_1, ..., \mathbf{R}_N) \propto \pi(\mathcal{A}^*) \pi(\boldsymbol{\rho} | \mathcal{A}^*) \frac{1}{Z_{n^*}(\alpha)} \exp \left\{ -\frac{\alpha}{n^*} \sum_{j=1}^N d_{\mathcal{A}^*}(\mathbf{R}_j, \boldsymbol{\rho}) \right\} \cdot \prod_{j=1}^N \left\{ U_{\mathcal{A} \setminus \mathcal{A}^*}(\mathbf{R}_j) 1_{\mathcal{P}_n}(\mathbf{R}_j) \right\},$$
(1)

which, by removing the terms not depending on any of the model parameters and by assuming the data are proper rankings, can be simplified to

$$P(\boldsymbol{\rho}, \mathcal{A}^* | \mathbf{R}_1, ..., \mathbf{R}_N) \propto \exp \left\{ -\frac{\alpha}{n^*} \sum_{j=1}^N d_{\mathcal{A}^*}(\mathbf{R}_j, \boldsymbol{\rho}) \right\} 1_{\mathcal{P}_{n^*}}(\boldsymbol{\rho}) 1_{\mathcal{C}}(\mathcal{A}^*).$$
 (2)

Note that, from the posterior distribution in (2), marginal posterior distributions of both model parameters, ρ and \mathcal{A}^* , can be easily derived. By inspecting the marginal posterior distribution of \mathcal{A}^* estimated by the variable selection model, one can then a posteriori select the items in \mathcal{A} that maximise the marginal posterior under all possible model reductions of dimension n^* , thus practically attaining variable selection as the MAP of \mathcal{A}^* . However, this model has much wider implications: for example, by inspecting the marginal posterior distribution of \mathcal{A}^* one can decide whether variable selection is appropriate to the data at hand (few items are clearly assigned rankings while the rest shows high uncertainty), or rather items are a posteriori ranked in blocks (several items share the same rank with large probability, and only a respective ordering between groups of items can be properly estimated). Scope of the simulation studies in Section 3 is to assess the correct behavior of the model in these different scenarios, together with its gain in efficiency in the large n context.

2.3. Metropolis-Hastings algorithm for inference in the lowBMM

In order to obtain samples from the posterior in equation (1), we set up a Markov Chain Monte Carlo (MCMC) algorithm, based on a Metropolis-Hastings scheme. The algorithm iterates between two steps: in one step the consensus ranking ρ restricted to the set \mathcal{A}^* is updated, and in the second step the set \mathcal{A}^* is updated given the current consensus ranking.

In the first step of the algorithm, we propose a new consensus ranking ρ' using the "leap-and-shift" proposal distribution described in [31]. The acceptance probability for updating ρ in the Metropolis-Hastings algorithm is

$$\min \left\{ 1, \frac{P_l(\boldsymbol{\rho}|\boldsymbol{\rho}')}{P_l(\boldsymbol{\rho}'|\boldsymbol{\rho})} \exp \left[-\frac{\alpha}{n^*} \left(\sum_{j=1}^N d_{\mathcal{A}^*}(\mathbf{R}_j, \boldsymbol{\rho}') - \sum_{j=1}^N d_{\mathcal{A}^*}(\mathbf{R}_j, \boldsymbol{\rho}) \right) \right] \right\}.$$
(3)

In equation (3) above, P_l denotes the probability mass function associated to moving from one n^* -dimensional ranking vector to another according to the leap-and-shift proposal. The parameter l denotes the number of items perturbed in the consensus ranking ρ to get a new proposal ρ' , and is used to tune the acceptance probability. To compute the distances restricted to \mathcal{A}^* , the \mathbf{R}_j 's needs to be updated so that they correspond to the items in the current set \mathcal{A}^* .

The second step of the algorithm updates the set \mathcal{A}^* . We propose a new set $\mathcal{A}^*_{\text{prop}}$ by perturbing $L \in \{1, ..., n^*\}$ elements in the current \mathcal{A}^* . The L items are swapped with L items from the set $\mathcal{A} \setminus \mathcal{A}^*$. The move from \mathcal{A}^* to $\mathcal{A}^*_{\text{prop}}$ is accepted with probability

$$\min \left\{ 1, \exp \left[-\frac{\alpha}{n^*} \left(\sum_{j=1}^N d_{\mathcal{A}_{\text{prop}}^*}(\mathbf{R}_j, \boldsymbol{\rho}) - \sum_{j=1}^N d_{\mathcal{A}^*}(\mathbf{R}_j, \boldsymbol{\rho}) \right) \right] \right\}. \tag{4}$$

Note that $d_{\mathcal{A}_{\text{prop}}^*}(\mathbf{R}_j, \boldsymbol{\rho}) = d_{n^*}(\mathbf{R}_j|_{\mathcal{A}_{\text{prop}}^*}, \boldsymbol{\rho}|_{\mathcal{A}_{\text{prop}}^*})$, i.e. the distance is computed on the restricted space of the current $\mathcal{A}_{\text{prop}}^*$. One consequence of this is deciding how to choose $\boldsymbol{\rho}|_{\mathcal{A}_{\text{prop}}^*}$. There are multiple ways of doing this, the most simple being to randomly perturb the current $\boldsymbol{\rho}$ from the first step of the algorithm to accommodate the new L items proposed for $\mathcal{A}_{\text{prop}}^*$. That is, given the current $\boldsymbol{\rho}$, we discard the ranks corresponding to the L items that were left out of $\mathcal{A}_{\text{prop}}^*$, and randomly assign ranks for the new items (in the restricted space of dim n^*).

This way of defining the acceptance probability does not perform variable selection on the top only. Instead, we will be able to pick out the n^* items where the assessors agree the most. The algorithm will accept items where the distance between the ranks and the consensus is the smallest, i.e. we get a type of consensus constrained to a specific number of items. The MCMC algorithm described above is summarized in Algorithm 1.

Algorithm 1: MCMC scheme for inference in lowBMM

2.4. Off-line estimation of α

While we have so far assumed that α is fixed and known, we would still need an estimation of its most reasonable value when we are given a new ranking dataset. We propose one possible method for estimating such a value, inspired by [23].

As α describes how closely the rankings are distributed around the common consensus, or in other words, how similar the individual rankings are to each other, we can assume that a higher α indicates a higher "similarity" between assessors. Therefore, when assuming that the individual rankings of the assessors are drawn from a Mallows with parameter α , a higher α results in a lower mean distance between the assessors. To estimate α we assume that the mean distance between assessors for a ranking dataset with n items ranked by N assessors should resemble the mean distance of a simulated ranking dataset with the same dimensions, generated by drawing independent samples from the Mallows distribution. Precisely, suppose we want to estimate α from a ranking dataset with n items ranked by N assessors: we can then generate several ranking datasets of dimension (N, n) over a grid of α_0 values, $\mathbf{R}_1^{\alpha_0}, \ldots, \mathbf{R}_N^{\alpha_0}$ (the chosen consensus ranking $\boldsymbol{\rho}_0$ does not matter). Then, we calculate the mean pairwise distance between assessors for each simulated dataset (i.e. for every α_0), defined as:

$$\bar{d}_{\alpha_0} = \frac{1}{N(N-1)} \sum_{j=1}^{N} \sum_{k \neq j} d(\mathbf{R}_j^{\alpha_0}, \mathbf{R}_k^{\alpha_0}).$$
 (5)

Finally, we compute the same mean distance between assessors as in (5) for the dataset we are interested in, and choose the α_0 value where the two distance measures intersect.

The approach to estimate α described so far works for a complete ranking dataset where we assume that all n items are ranked according to independent draws from the Mallows distribution. However, when using the lowBMM, we will be assuming that only n^* items are ranked according to a Mallows model. Hence, when using the method described above we will need to re-scale the estimated α from dimension (N,n) to dimension (N,n^*) . Let $\hat{\alpha}_n$ be the optimal α_0 value estimated from the datasets of dimension (N,n), as described above. We can then re-scale $\hat{\alpha}_n$ to obtain the optimal $\hat{\alpha}_{n^*}$ value in dimension n^* by matching the terms in the exponent in the Mallows model:

$$\hat{\alpha}_{n^*} = \hat{\alpha}_n \frac{n}{n^*} \frac{\max_{d_{n^*}}}{\max_d}$$

where \max_{d_n} (respectively $\max_{d_{n^*}}$) is the maximum attainable footrule distance between two rankings in dimension n (respectively n^*). The method is assessed in a simulation study described in Section 3.6.

3. Simulation experiments

This section describes how lowBMM performs under different data generating processes. The variable selection procedure provides a posterior distribution for the consensus ranking in a reduced dimension, and the type of distribution obtained in turn depends on the data generating process. Therefore, inspecting the solution provided by lowBMM under different scenarios allows us to understand the data structure and patterns in real-life situations.

First, we consider a top-rank data generating process, where only a subset of the items is ranked, and assigned the top ranks in reduced dimension, while the rest is noisy: this scenario results in a top-rank solution, i.e., lowBMM correctly selects the top-items following a rank model. Second, we generate data where items are consistently awarded ranks in a specific order: this results in a rank-consistency solution, i.e., items that can be ordered are selected and top-ranked. We also test the method's robustness to the noise level in the data, and we finally provide a performance assessment of the off-line estimation of α .

3.1. Top-rank data generating process: toy example

In this simulation study, we consider a group of N=50 assessors, and n=20 items. n^* items were given ranks sampled from the Mallows model: $R_j|\mathcal{A}^* \sim \text{Mallows}(1:n^*,\alpha)$, while the rest of the items were randomly assigned ranks; $R_j|\mathcal{A} \setminus \mathcal{A}^* \sim \mathcal{U}(\mathcal{P}_{n^*+1,\ldots,n})$. We experimented by varying the two tuning parameters introduced in Section 2.3: L, i.e., the number of items perturbed for proposing \mathcal{A}^* , and l, i.e., the number of items perturbed for proposing the consensus ρ . Both L and l were distributed over a grid $(L,l) \in [1,2,3] \times [1,2,3]$.

We first ran the method with the correct n^* , where the algorithm looks for the top n^* items, which were essentially the only items with clear ranks in the data. Heatplots of the marginal posterior distributions of ρ for the experiments with different tuning parameters can be seen in Figure 1 with $\alpha=3$. The choice of tuning parameters does not seem to affect the error. This is true also when varying the value of α (see S1 with $\alpha=10$ in the supplementary material).

We also inspected how the solution changed when varying α . The α parameter regulates how much the assessors agree with each other on the ranking of the items: a large α means a better agreement between the assessors, and a lower α means less agreement. So, when α is large, the items distributed according to the Mallows are easier to pick out, making it less likely that other items are accepted in the proposal set. This is evident in the distribution of the bars on the top of the plots in Figure 2, where the larger α value shows less variability in the selected items. Moreover, when the data is "easier", the algorithm converges much more quickly to the correct set. The bottom items (whose ranks are essentially noise) are clearly distributed on the bottom for $\alpha=10$, while there is a bit more uncertainty for $\alpha=3$, as expected.

It is also worth exploring the acceptance probability for the two parameters estimated in the MCMC, ρ and \mathcal{A}^* , as shown in Figure 3. It seems that for $\alpha = 3$ and $n^* = 8$ (n = 20 and N = 50 in this scenario), the acceptance

probability for ρ increases with increasing L, while it decreases with increasing l; the latter behavior is expected, while the former is less trivial to understand. For what concerns \mathcal{A}^* , the acceptance probability decreases with increasing L, and it seems to not be much affected by the leap size l, which are both quite natural behaviors. However, these conflicting trends make it challenging to choose a combination of tuning parameters that results in a chain that explores the space well.

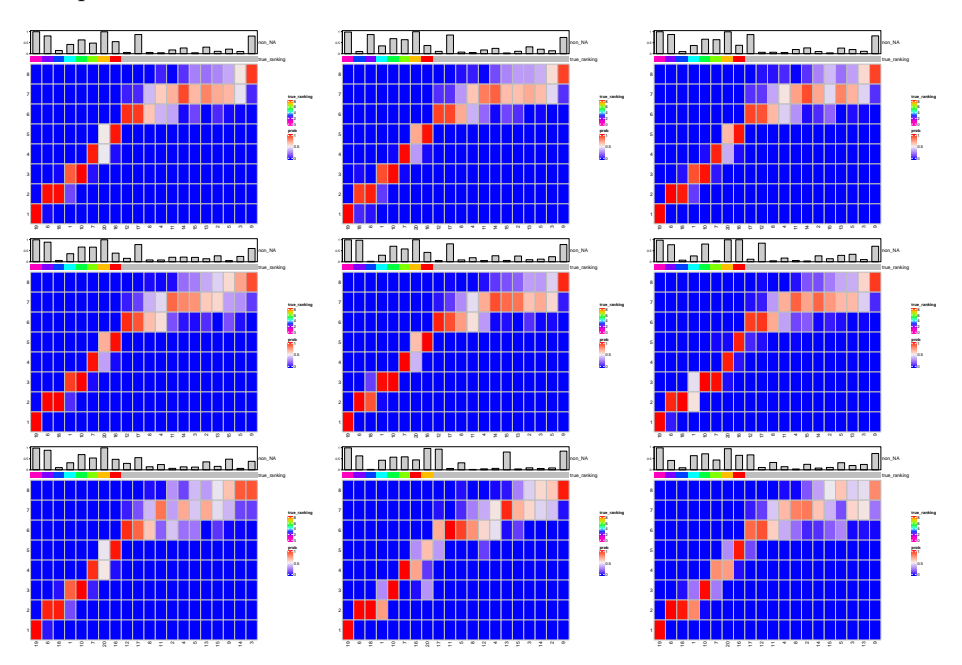


Figure 1: Results from simulation experiments described in section 3.1, marginal posterior distribution of ρ . From left to right, l=1,2,3, and from top to bottom L=1,2,3; $\alpha=3$, the true rank is indicated as a rainbow grid, and the bar plot indicates the proportion the items were selected in \mathcal{A}^* over all MCMC iterations.

In addition to running the analysis with the correct n^* , we tested the algorithm by assuming a different n^* than what was used when simulating the data. This means that the algorithm assumes there are either more or fewer items to be looked for, which is a quite realistic scenario in many practical applications. In Figure 4, left panel, we see that assuming $n^*_{\text{guess}} < n^*$ yields a clustered structure, thus implying that the best lower-dimensional solution of higher-dimensionally ranked data is consistent with a partial ordering, also called "bucket solution" [12]. On the other hand, assuming $n^*_{\text{guess}} > n^*$ yields a top-rank solution (Figure 4, right panel), as the algorithm seems to be able to indirectly suggest the true n^* by showing a much larger uncertainty around the items ranked with larger values than n^* . Overall, when $n^*_{\text{guess}} > n^*$, the posterior distribution of ρ is more accurate, in that it gives larger probabilities for

the top ranks to the correct items. Similar trends were obtained in simulation studies with varying α and the tuning parameters l and L, see S2, S3, S4 and S5 in the supplementary material.

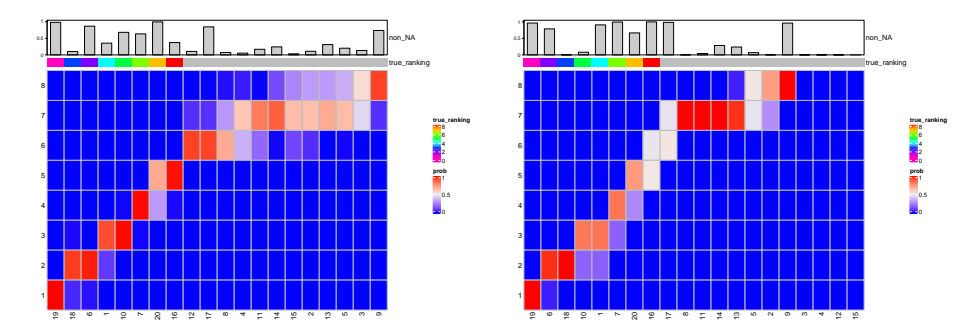


Figure 2: Results from simulation experiments described in section 3.1, marginal posterior distribution of ρ . Left $\alpha = 3$, right $\alpha = 10$. Tuning parameters: L = 1 and l = 2.

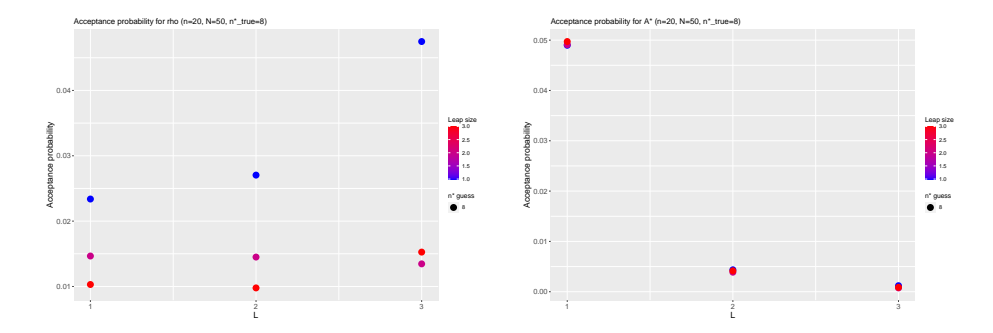


Figure 3: Results from simulation experiments described in section 3.1, acceptance probabilities in the simulated scenario when $n^* = 8$, $\alpha = 3$. Left: acceptance probability for the consensus ranking ρ . Right: acceptance probability for the set of selected items \mathcal{A}^* . The x-axis corresponds to varying L = [1, 2, 3], while the colors correspond to varying l = [1, 2, 3].

As a final check of the performance of lowBMM, we also would like to ensure that the method is consistent with the full model, i.e., with the Bayes Mallows for complete data as introduced in [31]. To this aim, we ran the full Bayes Mallows model as well as the variable selection lowBMM on the same simulated dataset. For a comparison of the marginal posterior distribution obtained on the reduced set of items with the lowBMM to the one obtained with BayesMallows on the complete set of items, see Figure 5, right and left panel, respectively. Both models show similar results for the top items, with the full model being slightly more certain in its top ranks. The noisy items seem to be randomly distributed on the bottom in the full model, while in lowBMM they are assigned

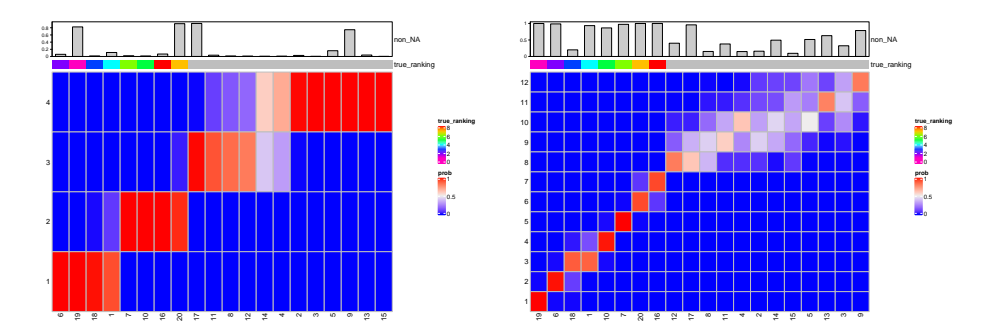


Figure 4: Results from simulation experiments described in section 3.1, marginal posterior distribution of ρ with $n^* = n^*_{\text{guess}}$. Left $n^*_{\text{guess}} = 4$, right $n^*_{\text{guess}} = 12$. Other parameters: $n^*_{\text{true}} = 8$, $\alpha = 3$, L = 1 and $l = \text{round}(n^*_{\text{guess}}/5)$.

the bottom three ranks, if any.

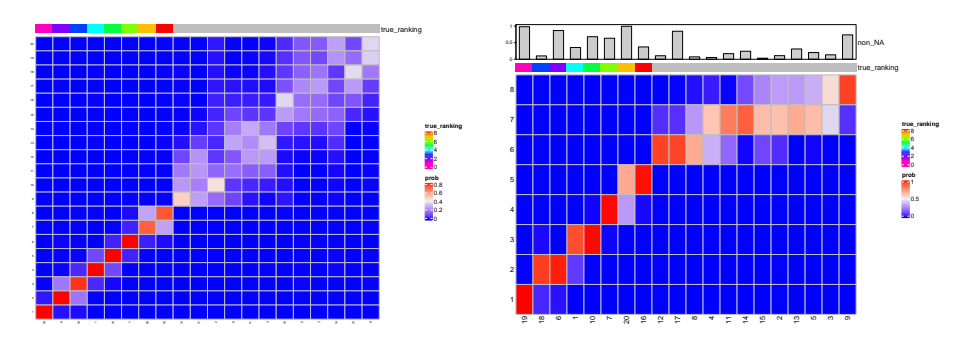


Figure 5: Results from simulation experiments described in section 3.1: comparison of the BayesMallows model on the complete set of items to lowBMM with n^* items. Probability of items being ranked 1,...,n on the left and $1,...,n^*$ on the right, with fixed $\alpha=3$. Tuning parameters for the right hand plot: L=1, l=2. The true rank is indicated as a rainbow grid, and the bar plot indicates the proportion the items were selected in \mathcal{A}^* over all MCMC iterations.

3.2. Top-rank data generating process: larger dimension example

In order to test the method in a more realistic scenario, we simulated the data in a dimension closer to one of the purposed applications. The present simulation study aims to investigate the method performance on a larger dataset when using the same data generation process as in Section 3.1. We set the total number of items to n = 1000, $n^* = 50$ and the number of assessors to N = 50. For the tuning parameters: we fixed $l = \text{round}(n^*/5)$, as suggested in BayesMallows and after some tuning (we have shown in Section 3.1 that this parameter does

not affect the results as much as L) and varied L = [1, 2, 3, ..., 15]. The results showed a clear indication that smaller L results in a lower error in terms of how many items were correctly ranked (ref. S7 in the supplementary material). The method was able to select more than 75% of the items from the true \mathcal{A}^* as well as many of their respective rankings (the true $\rho|_{\mathcal{A}^*}$), with tuning parameters L = 1 and $l = \text{round}(n^*/5)$. The posterior of $\rho|_{\mathcal{A}^*}$ can be seen in the left plot of Figure 6, where most of the items in the true selection are distributed at the top, with the uncertainty increasing for the bottom items (items not in the top n^*). The trace plot on the right in Figure 6 demonstrates convergence, with most top-ranked items clearly converging to one final rank, and only a few competing for the same rank throughout the chain. This "competing" behavior should to some degree be expected, however we noticed it to be enhanced by increasing the tuning parameter L (see S6 in the supplementary material), further supporting the decision to keep L small.

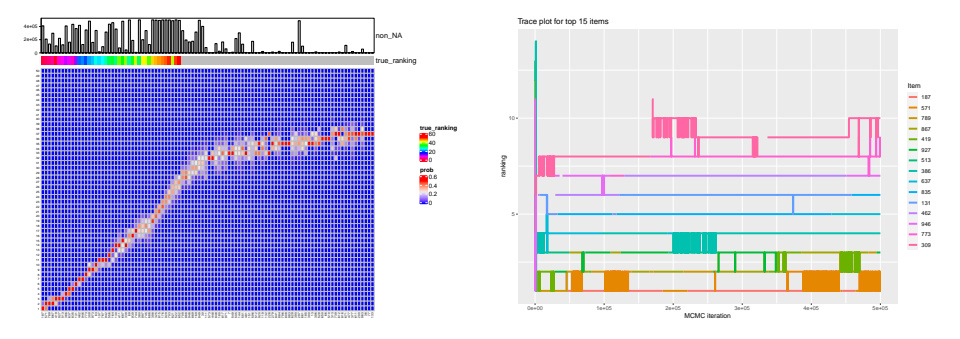


Figure 6: Results from simulation experiments described in section 3.2, for $\alpha = 10$, L = 1, l = 10. Left: probability of the top-100 items items being ranked $1, ..., n^*$. Right: trace plot of the top-15 items being ranked $1, ..., n^*$.

3.3. Robustness to noise experiment

The simulated data experiments have so far been somewhat easy for the method to handle, especially in terms of noise: we only tested a varying degree of agreement among the top-ranked items by varying α . To test the method's robustness to noise, we performed another simulation experiment where we generated data as previously and then added an increasingly strong random perturbation of the rankings. We therefore first simulated datasets as in Section 3.1 ($n^* = 8$ items sampled from the Mallows, out of a total n = 20 items for N = 25 assessors), and then iteratively swapped the rankings of items in the top n^* (sampled from the Mallows) with items ranked below. The procedure we used can be described as follows: at level 1, we started with the bottom item in the true set \mathcal{A}^* (the item whose generating rank is n^*), and swapped the rank for that item with the rank of an item outside of the true set, for 90% of the assessors. This was repeated a total of four times (i.e. at level 4, the ranks of four items in the true

set were swapped with items from the outside). The tuning parameters were distributed over the grid $(L, l) \in [1, 2, 3] \times [1, 2, 3]$. The results can be seen in Figure 7, which displays boxplots of the footrule distance between the true and the posterior ρ (normalized by the number of correct items in \mathcal{A}^*). The results generally show a very good performance of the method even with an increasing level of the perturbation. The figure also suggests that a lower L is more robust to noise, while the leap size l has very little effect.

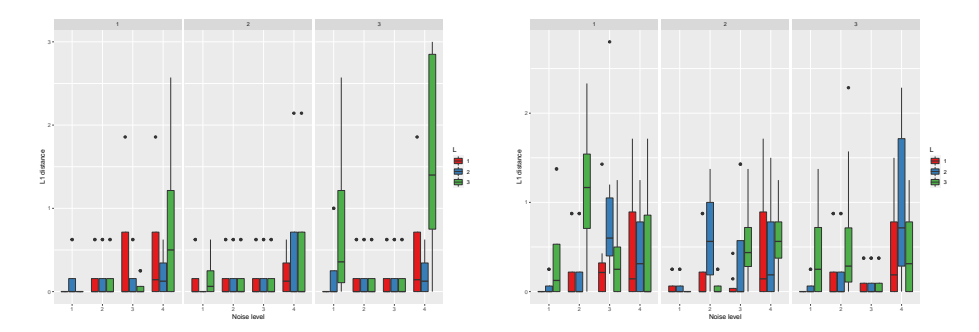


Figure 7: Results from simulation experiments described in section 3.3: boxplot of the footrule distance between the true and the estimated ρ , normalized by the number of correct items. From left to right: $\alpha = 3$ and $\alpha = 10$. Each subplot from left to right displays the tuning parameter l = [1, 2, 3] and the color of the bars indicate the tuning parameter L = [1, 2, 3].

3.4. Rank consistency experiment

We performed another simulation study with a different data generation process to see whether our method can select consistently ranked items even if not necessarily top-ranked. The setting is the following: items in A^* were given a respective ranking sampled from a Mallows model in dimension n^* ; then, the same items were assigned a random ranking in dimension n in their respective positions; finally, the rest of the items had randomly assigned ranks. Therefore, items in the true A^* were always ranked in a certain order for each assessor, however their specific ranks were not consistent. In the data generating process, we experimented with changing the number of items being given the consistent ranks, n^* , as well as the level of spread (or noise) in the data sampled from the Mallows, α . We always set the total number of items to n=20 and the number of assessors N = 50. We see in the two top plots in Figure 8 that there is much more uncertainty in the ranks with $\alpha = 0.5$, while more or less none with $\alpha = 10$, which is expected. What is more interesting is the performance of the method: while the upper two plots look somewhat messy compared to the two bottom ones, there is still most weight given to the correct items (looking at the bar plots at the top). The ordering of the items is in all cases consistent with the solution, even in the cases with a high level of noise.

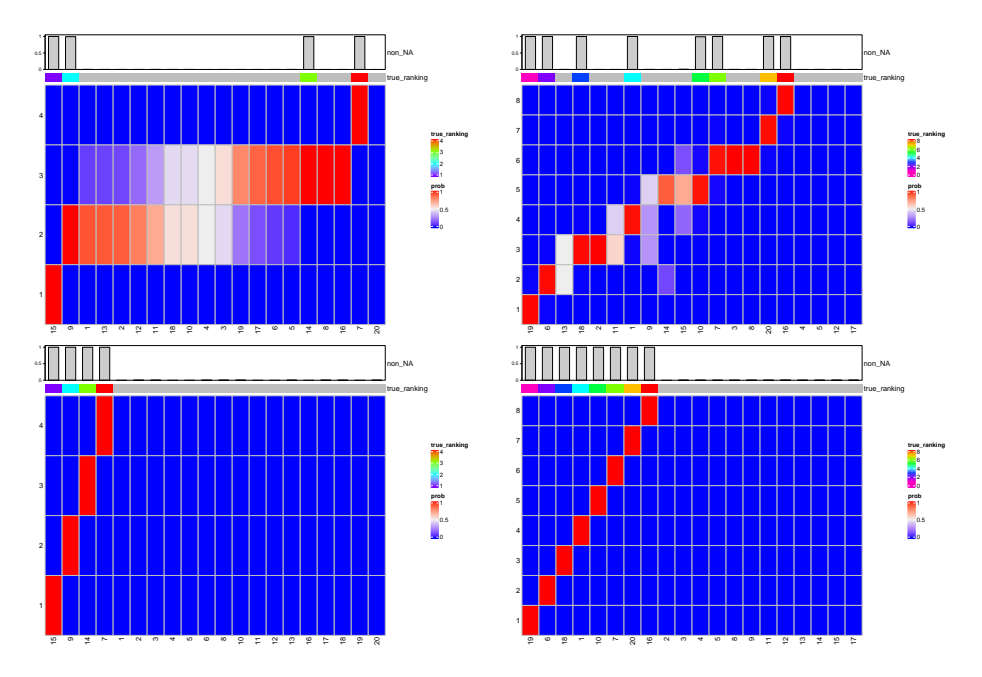


Figure 8: Results from simulation experiments described in section 3.4: probability of items being ranked $1, ..., n^*$. Left to right: $n^* = 4$ and $n^* = 8$; top to bottom: $\alpha = 0.5$ and $\alpha = 10$. In all cases we set L = 1 and $l = \text{round}(n^*/5)$.

3.5. Comparison with the Bayesian Mallows Model (BMM)

We performed another comparison between the analysis on the complete set of items with the Bayesian Mallows model (BMM), and the analysis on the reduced set of items with the variable selection procedure (lowBMM), on a larger example. Figure 9 demonstrates that the variable selection outperforms BMM in terms of accuracy and stability in the two data generating examples. For the toprank data generation, lowBMM converges to the solution with fewer iterations, while BMM reaches the solution at a later stage. This shows the consistency of lowBMM, as we obtain the same solution as for the full set, however in the correct reduced dimension and with lower computational demands. For the rank-consistency data scenario, lowBMM outperforms BMM. While lowBMM converges to the solution after 3000 iterations, BMM exhibits an oscillating behaviour, and it never manages to reach convergence. This last simulation example further shows the flexibility in the variable selection procedure under different data generating procedures, even in a high-dimensional setting with basically no possible competitor.

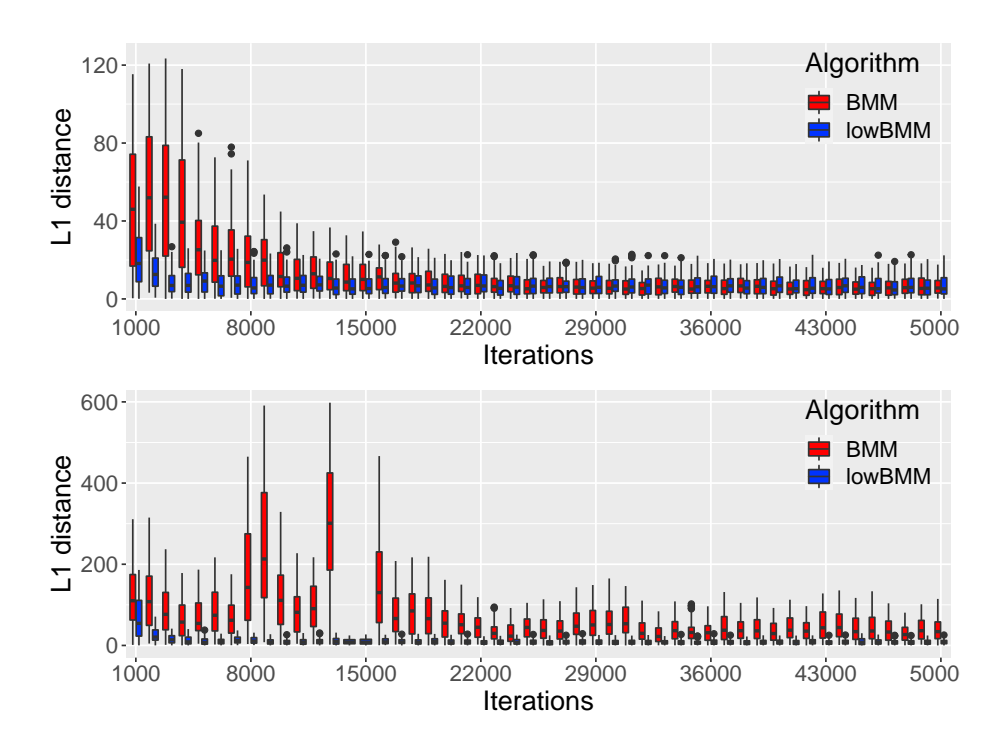


Figure 9: Results from simulation experiments described in section 3.5: boxplot of the footrule distance between the true and the estimated ρ normalized by the number of correct items at each MCMC iteration for the full BMM (red) and lowBMM (blue) models. Top: top-rank simulation example with $\alpha=5$; bottom: rank-consistency simulation example with $\alpha=2$.

3.6. Off-line estimation of α

Finally, we also aimed at testing the approach described in Section 2.4 for the off-line estimation of α in a simulation setting with a data generating process as previously used. We therefore generated datasets with varying dimensions (N,n), where $n^* = \text{round}(n/3)$ items were sampled from the Mallows model with a fixed α_{true} , and the rest of the items were sampled from a uniform distribution. For each dataset in a given dimension, we ran the estimation procedure of Section 2.4 by generating datasets of equal dimension over a grid of α_0 values, and computed the mean distance between assessors of each dataset. Finally, we obtained the final estimate $\hat{\alpha}_n^*$ by determining the intersection between the distance measure for the simulated datasets and the distance measure for the dataset generated from α_{true} , in each dimension. Performance of the estimation procedure can be inspected in Table 1, where the method stability is demonstrated even for increasing n.

n	n^*	$\hat{\alpha}_{n^*}$
20	7	2.18
150	50	2.23
500	167	2.24
1000	333	2.21

Table 1: Results from simulation experiments described in section 3.6, for testing the off-line estimation of α as described in Section 2.4 with $N=50,\ n^*=\mathrm{round}(n/3)$ and $\alpha_{\mathrm{true}}=3$ for all scenarios.

4. Application to RNA-seq data from ovarian cancer patients

In this section we describe the application of the lowBMM method on RNAseq data from TCGA ovarian cancer patients. The data was downloaded from CGHub (www.cghub.ucsc.edu) and converted to FASTQs, all samples were processed similarly aligning reads to the hg19 genome assembly using Map-Splice [32]. Gene expression was quantified for the transcript models corresponding to the TCGA GAF 2.13, using RSEM4 and normalized within-sample to a fixed upper quartile [20]. Gene level expression data was available at the TCGA Data Portal (https://tcga-data.nci.nih.gov/tcga/), and correspond to the data used in [14].

Serous ovarian tumors share similar genetic origin and features with basal-like breast cancers [6]: both are difficult-to-treat cancer types, and they are highly commonly characterized at the molecular level, especially for what concerns mutations (with TP53 being the most frequent example). Massive whole-genome data analyses are therefore key to understanding individual tumor biology for these cancer types. This is the main motivation for focusing on RNAseq data from serous ovarian tumors, as selecting basal-like breast cancer patients would require an additional subtyping preprocessing step that we would like to avoid. Additionally, since our method assumes complete data, pre-processing steps included keeping only the items (genes) with less than 50% missing values: all of these missing values were imputed using k-nearest neighbor averaging [30]. This resulted in a final dataset with N=265 patients and n=15348 genes.

For running our lowBMM method, we set $n^* = 500$, l = 20 and L = 1 (tuning parameters were set based on the simulation studies as demonstrated in Section 3.1). We also performed an off-line estimation of α on the experimental dataset, as described in Section 2.4, which resulted in setting $\alpha = 10$. Due to the high dimensionality of the data, we ran two chains, each with $M = 5 \times 10^6$ MCMC iterations on a big memory HPC server. We discarded the first 5×10^4 iterations as burn-in in both chains before merging them for post-processing.

The two chains agree on 83% of the items in the final selection \mathcal{A}^* , although they did not converge to the exact same distribution for ρ . This might be due to a combination of several factors: first, the stickiness of the method (the MCMC)

being defined on a discrete state space, it encounters difficulties in "switching rank" close to convergence); then, the tuning parameters, which are difficult to set at best as their optimal behavior is often conflicting with one another; finally, the n^* value used in the analysis, which might be too low. Concerning the latter aspect, we remark that the simulation study in Section 3.1 suggested that running lowBMM with a smaller n^* compared to the "truth" might make it more difficult for the method to converge to the true ρ . Moreover, during the off-line estimation of α , we estimated the n^* that best fits the experimental data to $n^* \approx 2400$. However, we kept the final $n^* = 500$ value as it is more suited to allow results interpretability, and as it also allows the MCMC to perform a good exploration of the state space given the current computational capacity.

To gain insight on the results provided by lowBMM on the experimental dataset, we computed a refined gene selection to be used in a Gene Set Enrichment Analysis (GSEA) [26,29], to verify whether the method could identify common genes related to cancer. To this aim, we computed $P(x \in \text{top-}K|x \in \mathcal{A}^*)$ for all the items x for various choices of K, with a threshold for the lower items: genes that had probability less than 0.1 of being in the different K-sets were dropped. This resulted in the violin plots shown in Figure 10, left panel: this plot indicates that K = 75 is a good choice for allowing many genes to have a quite large probability. We therefore further inspected the probability distribution of the probabilities included in the top-75 violin plot, by drawing an histogram of the same probabilities (Figure 10, right panel): this second plot allowed us to select a cut-off point of c = 0.77 for the top-75 probability, thus resulting in a final selection of n' = 63 genes such that $A' = P(x \in \text{top-}75|x \in A^*) > c$ for each gene x in the refined selection.

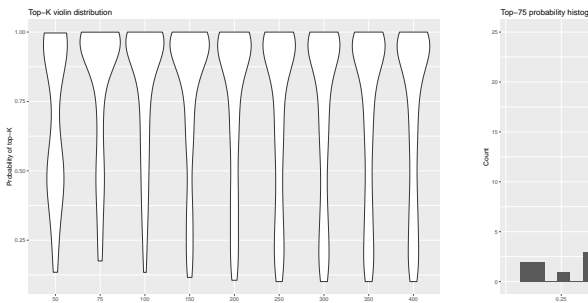
Figure 11 shows that the items in the refined selection \mathcal{A}' are almost always selected, even if they sometimes "compete" for some of the available ranks: this effect might be due to the two chains converging to slightly different ρ , but highly similar \mathcal{A}^* . There is overall more variability in the rankings of the items as compared to the simulation studies, which is to some degree expected in experimental data with a higher degree of noise. Higher variability in the ranks was also typical for the simulation studies where $n_{\text{guess}}^* << n_{\text{true}}^*$ (see Figure 5).

The GSEA indicated that the lowBMM identified known genes involved in cell differentiation and cancer development. The top-ranked genes were enriched in pathways such as cell differentiation, morphogenesis and developmental processes (Table 2), suggesting a role in the deregulation of cellular identity essential for cancer development.

The computations were performed on resources provided by UNINETT Sigma2, the National Infrastructure for High-Performance Computing and Data Storage in Norway.

5. Discussion

In this paper, we have developed a novel rank-based unsupervised variable selection method for high-dimensional data. The method extends the applicability



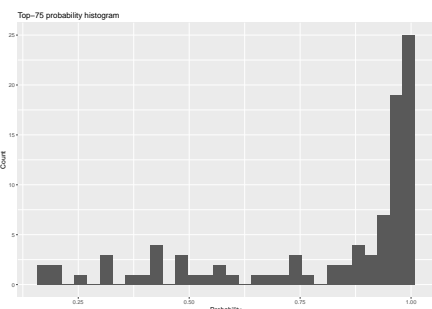


Figure 10: On the left: violin plots of $P(x \in \text{top-}K|x \in \mathcal{A}^*)$ for items x for various K. On the right: histogram of $P(x \in \text{top-}75|x \in \mathcal{A}^*)$ for items x. The following parameters are fixed: $\alpha = 10$, L = 1, l = 10.

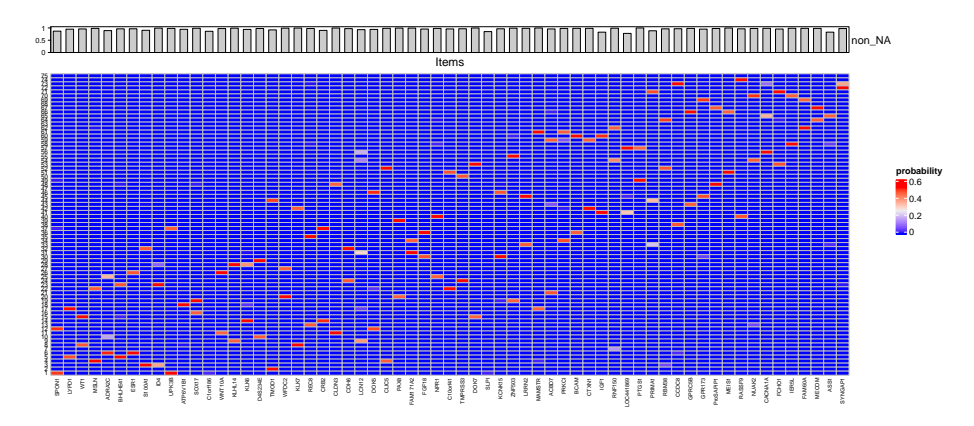


Figure 11: Posterior of $\rho|_{\mathcal{A}'}$. The bars on top indicate the proportion the item was selected over all MCMC iterations, with the following fixed parameters: $\alpha = 10, L = 1, l = 10.$

of the Bayesian Mallows ranking model to unprecedented data dimensions and provides a much better modeling approach. Indeed, an important advantage of the variable selection procedure is the ability to distinguish relevant genes from the background ones, and to provide an estimate of the relative importance of the selected relevant genes. Furthermore, the variable selection procedure is able to work in high-dimensional settings where the number of items is $n >> 10^3$, with no competitor model for ranking data capable of scaling to such setting.

Simulation studies showed that the method performs well on datasets of varying sizes and under varying data generating procedures. We applied the proposed model to RNAseq data of ovarian cancer samples from TCGA. Although we consider a cancer genomics application, the methodological contribution given in this paper is very general, and can thus be applied to any high-dimensional setting with heterogeneous rank data.

Gene Set Name	# Genes in Gene set	# Genes in overlap	p-value
Regulation of cell differentiation (GOBP)	1618	16	2.59E-9
Regulation of multicellular organimsal development (GOBP)	1397	13	2.05E-7
Regulation of anatomical structure morphogenesis (GOBP)	1006	11	4.17E-7
Positive regulation of developmental process (GOBP)	1284	12	6.17E-7
Positive regulation of cell differentiation (GOBP)	844	10	7.2E-7
Response to endogenous stimulus (GOBP)	1624	13	1.12E-6
Cellular response to nitrogen compound (GOBP)	698	9	1.37E-6
Sensory organ development (GOBP)	534	8	1.84E-6
Animal organ morphogenesis (GOBP)	1025	10	4.08E-6
Striated muscle cell differentiation (GOBP)	269	6	4.12E-6

Table 2: Overview of top-10 gene sets from GSEA for the selection \mathcal{A}' , $|\mathcal{A}'| = 63$.

Throughout this work, we have assumed that the number of relevant items to be selected, n^* , is known. This is reasonable in many practical problems where a specific n^* can be tuned according to the research questions/demands or has to be decided according to computational capacity. Simulation studies showed that assuming $n^*_{\rm guess} << n^*_{\rm true}$ might pose problems in high-dimensional settings, and therefore the joint estimation of this parameter as part of the existing hierarchical framework constitutes a very interesting direction for future research.

The current version of lowBMM works under several assumptions: no handling of missing data, no clustering, fixed scale parameter α , all aspects which we plan to implement in future versions of the method. The somewhat challenging procedure of choosing the tuning parameters l and L might be solved with an adaptive MCMC and would allow the algorithm to explore the space more thoroughly. We leave this task for future consideration.

To our knowledge, no rank-based unsupervised variable selection procedure that is capable of scaling to the common data dimensions in -omics applications currently exists.

References

- [1] Bahman Afsari, Ulisses Braga-Neto, and Donald Geman. Rank discriminants for predicting phenotypes from RNA expression. *The Annals of Applied Statistics*, 8, 2014.
- [2] Aman Agrawal, Alec M. Chiu, Minh Le, Eran Halperin, and Sriram Sankararaman. Scalable probabilistic PCA for large-scale genetic variation data. *PLOS Genetics*, 16(5):1–19, 2020.
- [3] Ludmil Alexandrov, Serena Nik-Zainal, David Wedge, Peter Campbell, and Michael Stratton. Deciphering signatures of mutational processes operative in human cancer. *Cell reports*, 3:246–259, 2013.
- [4] Mayer Alvo and Philip L.H. Yu. Statistical Methods for Ranking Data. Frontiers in Probability and the Statistical Sciences. Springer, New York, NY, USA, 2014.

- [5] Bradley Barney, Federica Amici, Filippo Aureli, Josep Call, and Valen Johnson. Joint Bayesian modeling of binomial and rank data for primate cognition. *Journal of the American Statistical Association*, 110:00–00, 2015.
- [6] Colin B Begg, Megan S Rice, Emily C Zabor, and Shelley S Tworoger. Examining the common aetiology of serous ovarian cancers and basallike breast cancers using double primaries. *British Journal of Cancer*, 116(8):1088–1091, 2017.
- [7] Charles Bouveyron, Pierre Latouche, and Pierre-Alexandre Mattei. Bayesian variable selection for globally sparse probabilistic PCA. Electronic Journal of Statistics, 12(2):3036 – 3070, 2018.
- [8] Peter Bühlmann and Sara van de Geer. Statistics for high-dimensional data. Springer Series in Statistics. Springer, Heidelberg, Germany, 2011.
- [9] Can Cui, Susheela P. Singh, Ana-Maria Staicu, and Brian J. Reich. Bayesian variable selection for high-dimensional rank data. *Environmetrics*, pages 1–16, 2021.
- [10] Ke Deng, Simeng Han, Kate Li, and Jun Liu. Bayesian aggregation of order-based rank data. *Journal of the American Statistical Association*, 109(507):1023–1039, 2014.
- [11] Persi Diaconis. Group Representations in Probability and Statistics. volume 11 of Lecture Notes Monograph Series. Institute of Mathematical Statistics, Hayward, CA, USA, 1988.
- [12] Antonio D'Ambrosio, Carmela Iorio, Michele Staiano, and Roberta Siciliano. Median constrained bucket order rank aggregation. *Computational Statistics*, 34(2):787–802, 2019.
- [13] Katherine Hoadley, Christina Yau, Toshinori Hinoue, Denise Wolf, Alexander Lazar, Esther Drill, Ronglai Shen, Alison Taylor, Andrew Cherniack, Vésteinn Thorsson, Rehan Akbani, Reanne Bowlby, Christopher Wong, Maciej Wiznerowicz, Francisco Sánchez-Vega, Gordon Robertson, Barbara Schneider, Michael Lawrence, Houtan Noushmehr, and Armaz Mariamidze. Cell-of-origin patterns dominate the molecular classification of 10,000 tumors from 33 types of cancer. Cell, 173:291–304.e6, 2018.
- [14] Katherine Hoadley, Christina Yau, Denise Wolf, Andrew Cherniack, David Tamborero, Sam Ng, Mark Leiserson, Shubin Niu, Michael Mclellan, Vladislav Uzunangelov, Jiashan Zhang, Cyriac Kandoth, Rehan Akbani, Hui Shen, Larsson Omberg, Andy Chu, Adam Margolin, Laura van 't Veer, Nuria López-Bigas, and Lihua Zou. Multiplatform analysis of 12 cancer types reveals molecular classification within and across tissues of origin. Cell, 158(4):929-944, 2014.

- [15] Katja Ickstadt, Martin Schäfer, and Manuela Zucknick. Toward integrative Bayesian analysis in molecular biology. *Annual Review of Statistics and Its Application*, 5(1):141–167, 2018.
- [16] Trey Ideker, Janusz Dutkowski, and Leroy Hood. Boosting signal-to-noise in complex biology: prior knowledge is power. *Cell*, 144(6):860—863, 2011.
- [17] Valen Johnson, Robert Deaner, and Carel Schaik. Bayesian analysis of rank data with application to primate intelligence experiments. *Journal of the American Statistical Association*, 97:8–17, 2002.
- [18] Gary Koop and Dale J. Poirier. Rank-Ordered Logit Models: An Empirical Analysis of Ontario Voter Preferences. *Journal of Applied Econometrics*, 9(4):369–388, 1994.
- [19] Suprateek Kundu, Yichen Cheng, Minsuk Shin, Ganiraju Manyam, Bani K. Mallick, and Veerabhadran Baladandayuthapani. Bayesian variable selection with graphical structure learning: Applications in integrative genomics. PLOS ONE, 13(7):1–29, 2018.
- [20] Bo Li and Colin Dewey. RSEM: accurate transcript quantification from RNA-Seq data with or without a reference genome. *BMC bioinformatics*, 12:323, 2011.
- [21] Fan Li and Nancy R. Zhang. Bayesian variable selection in structured highdimensional covariate spaces with applications in genomics. *Journal of the American statistical association*, 105(491):1202–1214, 2010.
- [22] Qinghua Liu, Marta Crispino, Ida Scheel, Valeria Vitelli, and Arnoldo Frigessi. Model-based learning from preference data. *Annual Review of Statistics and Its Application*, 6(1):329–354, 2019.
- [23] Qinghua Liu, Valeria Vitelli, Carlo Mannino, Arnoldo Frigessi, and Ida Scheel. Pseudo-Mallows for efficient preference learning. *Manuscript in preparation*, 2021.
- [24] Robert D. Luce. Individual choice behavior: A theoretical analysis. Wiley, New York, NY, USA, 1959.
- [25] Colin L. Mallows. Non-null ranking models. Biometrika, 44(1/2):114–130, 1957.
- [26] Vamsi Mootha, Cecilia Lindgren, Karl-Fredrik Eriksson, Aravind Subramanian, Smita Sihag, Joseph Lehar, Pere Puigserver, Emma Nilsson, Martin Ridderstråle, Esa Laurila, Nicholas Houstis, Mark Daly, Nick Patterson, Jill Mesirov, Todd Golub, Pablo Tamayo, Bruce Spiegelman, Eric Lander, Joel Hirschhorn, and Leif Groop. PGC-1 alpha-responsive genes involved in oxidative phosphorylation are coordinately downregulated in human diabetes. *Nature genetics*, 34:267–73, 2003.

- [27] Robin L. Plackett. The analysis of permutations. *Journal of the Royal Statistical Society: Series C (Applied Statistics)*, 24(2):193–202, 1975.
- [28] Øystein Sørensen, Marta Crispino, Qinghua Liu, and Valeria Vitelli. BayesMallows: An R Package for the Bayesian Mallows Model. *The R Journal*, 12(1):324–342, 2020.
- [29] Aravind Subramanian, Pablo Tamayo, Vamsi K. Mootha, Sayan Mukherjee, Benjamin L. Ebert, Michael A. Gillette, Amanda Paulovich, Scott L. Pomeroy, Todd R. Golub, Eric S. Lander, and Jill P. Mesirov. Gene set enrichment analysis: A knowledge-based approach for interpreting genome-wide expression profiles. *Proceedings of the National Academy of Sciences*, 102(43):15545–15550, 2005.
- [30] Olga Troyanskaya, Michael Cantor, Gavin Sherlock, Pat Brown, Trevor Hastie, Robert Tibshirani, David Botstein, and Russ B. Altman. Missing value estimation methods for DNA microarrays. *Bioinformatics*, 17(6):520–525, 2001.
- [31] Valeria Vitelli, Øystein Sørensen, Marta Crispino, Arnoldo Frigessi, and Elja Arjas. Probabilistic preference learning with the Mallows rank model. Journal of Machine Learning Research, 18(1):5796—-5844, 2017.
- [32] Kai Wang, Darshan Singh, Zheng Zeng, Stephen Coleman, Yan Huang, Gleb Savich, Xiaping He, Piotr Mieczkowski, Sara Grimm, Charles Perou, James MacLeod, Derek Chiang, Jan Prins, and Jinze Liu. MapSplice: Accurate mapping of RNA-seq reads for splice junction discovery. Nucleic acids research, 38:e178, 2010.
- [33] Grace Yao and Ulf Bockenholt. Bayesian estimation of Thurstonian ranking models based on the Gibbs sampler. *British Journal of Mathematical and Statistical Psychology*, 52:79–92, 1999.
- [34] Philip Yu. Bayesian analysis of order-statistics models for ranking data. *Psychometrika*, 65(3):281–299, 2000.
- [35] Wanchuang Zhu, Yingkai Jiang, Jun S. Liu, and Ke Deng. Partition-Mallows model and its inference for rank aggregation. *Journal of the American Statistical Association*, pages 1–41, 2021.

Supplementary material

S1.

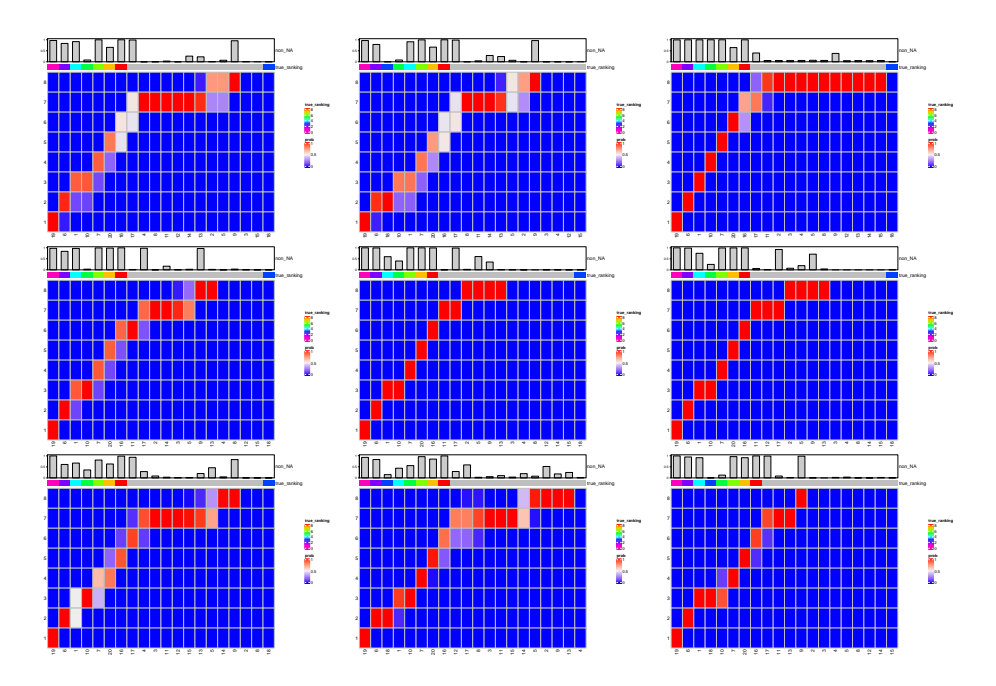


Figure 1: Top-rank data generating process with $n^*_{\text{true}} = n^*_{\text{guess}} = 8$. Each panel displays the probability of items being ranked $1, ..., n^*$. From left to right, l=1,2,3, and from top to bottom L=1,2,3; $\alpha=10$, the true rank is indicated as a rainbow grid, and the bar plot indicates the number of iterations the item was given a rank in the MCMC.

S2.

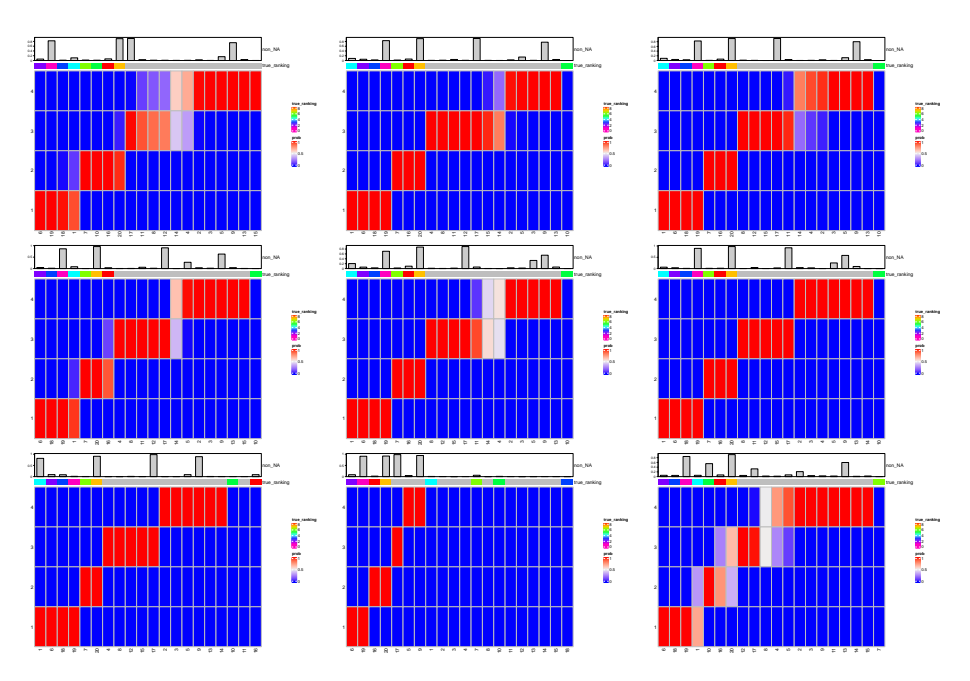


Figure 2: Top-rank data generating process with $n^*_{\text{true}} = 8$, $n^*_{\text{guess}} = 4$. Each panel displays the probability of items being ranked $1, ..., n^* - 4$. From left to right, l = 1, 2, 3, and from top to bottom L = 1, 2, 3; $\alpha = 3$, the true rank is indicated as a rainbow grid, and the bar plot indicates the number of iterations the item was given a rank.

S3.

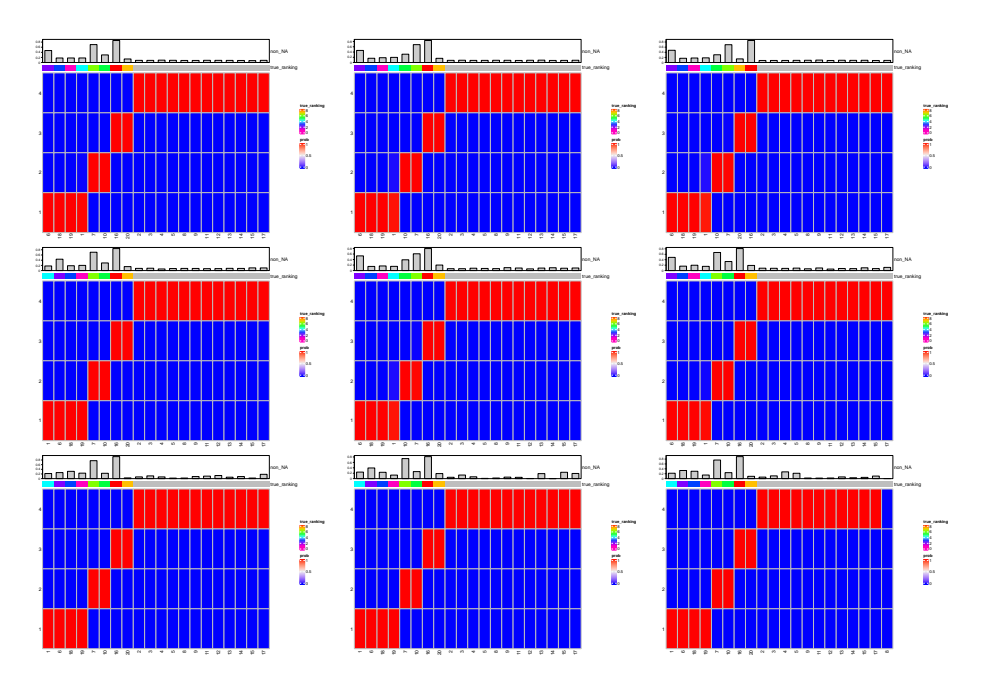


Figure 3: Top-rank data generating process with $n^*_{\text{true}} = 8$, $n^*_{\text{guess}} = 4$. Each panel displays the probability of items being ranked $1, ..., n^* - 4$. From left to right, l = 1, 2, 3, and from top to bottom L = 1, 2, 3; $\alpha = 10$, the true rank is indicated as a rainbow grid, and the bar plot indicates the number of iterations the item was given a rank.

S4.

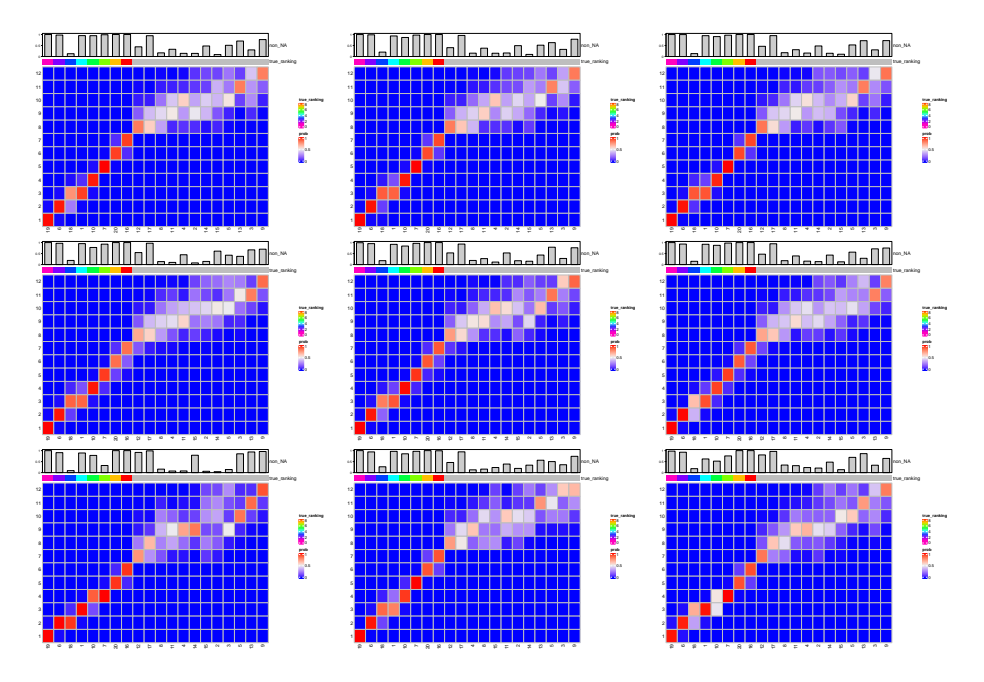


Figure 4: Top-rank data generating process with $n^*_{\text{true}} = 8$, $n^*_{\text{guess}} = 12$. Each panel displays the probability of items being ranked $1, ..., n^* + 4$. From left to right, l = 1, 2, 3, and from top to bottom L = 1, 2, 3; $\alpha = 3$, the true rank is indicated as a rainbow grid, and the bar plot indicates the number of iterations the item was given a rank in the MCMC.

S5.

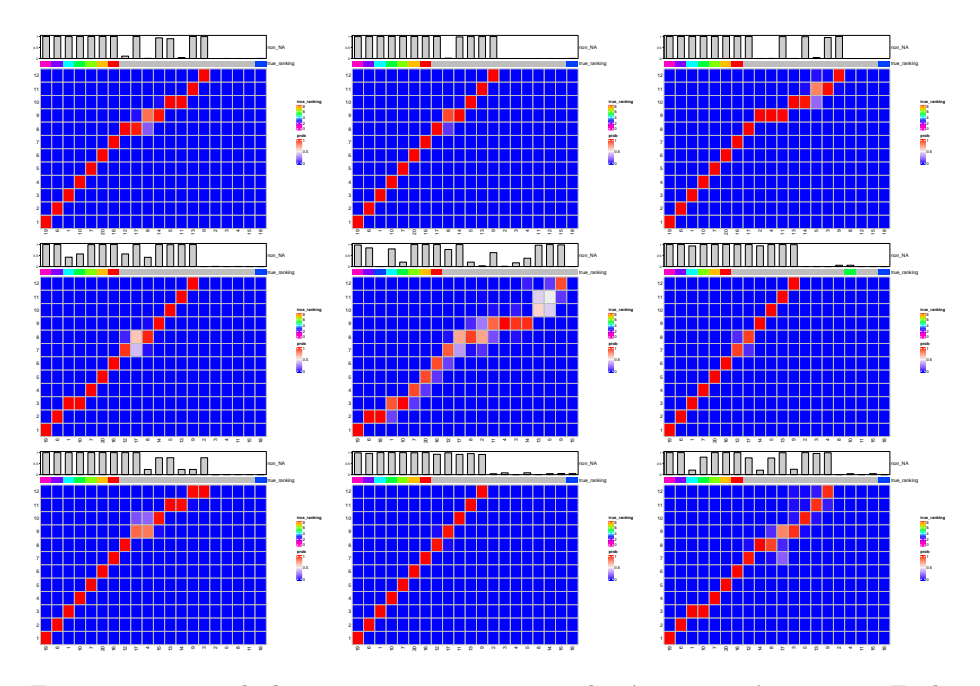


Figure 5: Top-rank data generating process with $n^*_{\text{true}} = 8$, $n^*_{\text{guess}} = 12$. Each panel displays the probability of items being ranked $1, ..., n^* + 4$. From left to right, l = 1, 2, 3, and from top to bottom L = 1, 2, 3; $\alpha = 10$, the true rank is indicated as a rainbow grid, and the bar plot indicates the number of iterations the item was given a rank in the MCMC.

S6.

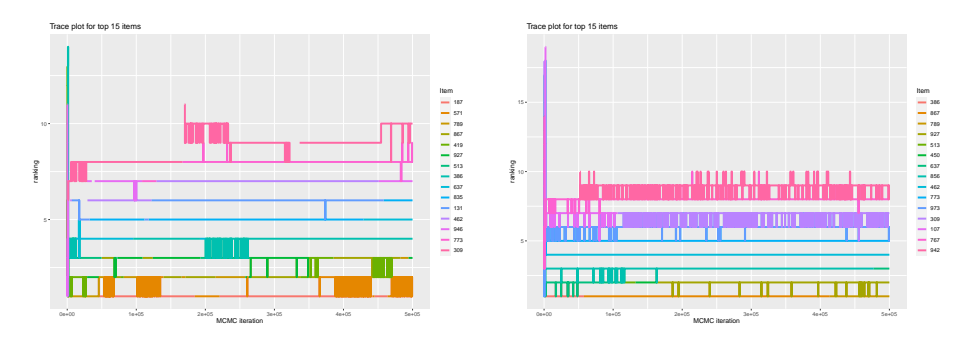


Figure 6: Top-rank data generating process with $n^* = 50$. Each panel displays the trace plot of the top 15 items being ranked $1, ..., n^*$ from left to right: L = 1 and L = 2 with $\alpha = 10$ and $l = \text{round}(n^*/5)$.

S7.

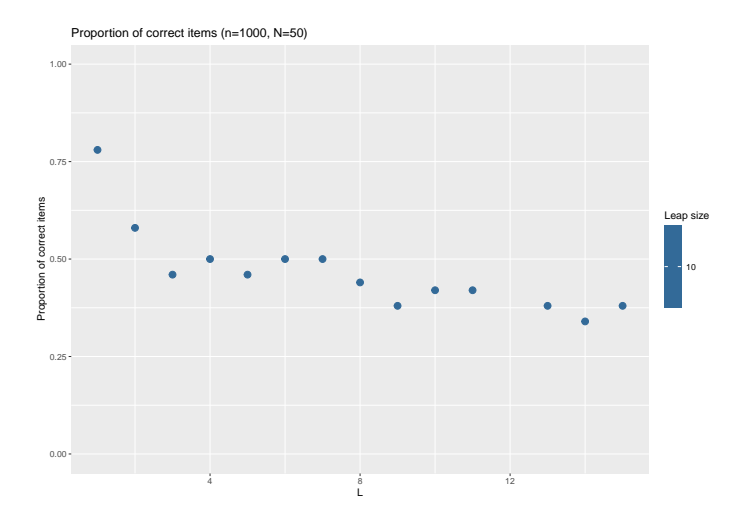


Figure 7: Top-rank data generating process with $n^* = 50$. Proportion of correct items in the posterior distribution of \mathcal{A}^* by varying L. $\alpha = 10$ and $l = \text{round}(n^*/5)$.